Synoptic changes in the deep rim current during stagnant hydrographic conditions in the Eastern Gotland Basin, Baltic Sea

Eberhard Hagen[*]
Rainer Feistel

Leibniz Institute for Baltic Sea Research,
Seestrasse 15, D–18119 Rostock–Warnemünde, Germany;

e-mail: eberhard.hagen@io-warnemuende.de

[*]corresponding author

Abstract

Hydrographic and current measurements are analysed for stagnant deep-water conditions over the south-eastern topographic flank of the Eastern Gotland Basin (EGB) in April 2000. Results suggest a prevailing barotropic motion mode on a synoptic scale of several days. Deep along-slope volume transports derived from subsurface current meter moorings are compared with those of the baroclinic fraction of geostrophic motions crossing the plane of a hydrographic section. This was aligned perpendicular to deep isobaths and was repeated 40 times with a time step of six hours. Changes in regional winds produced a quasi-ten day cycle in the filling level of the Baltic Proper. Associated wave-like fluctuations of the mass field propagated cyclonically with a velocity of about 0.04 m s^{-1} around the deep basin's rim. It is concluded that associated changes in deep volume transports result mainly from barotropically governed advection processes and that those of the baroclinic component of geostrophic currents provide a qualitatively and quantitatively quite inaccurate description of related transport fluctuations on a daily scale.

1. Introduction

Only exceptional strong inflow events are able to renew completely the water in deep basins of the Baltic Sea on a multi-year scale (Schinke

& Matthäus 1998). Such major inflows are separated by so-called stagnation periods lasting several years. The resulting overall residence time of Baltic deep water is about 20 years (Meier & Kauker 2003), but it exceeds 100 years in the absence of effective deep water intrusions. This follows from numerical circulation models as well as from the analysis of long-term hydrographic trends observed by the Baltic Monitoring Programme at central stations in deep Baltic basins (see Omstedt & Axell 1998, Feistel et al. 2006). In other words, the higher the frequency of such inflow events, the shorter the residence time of the water in the deep basins of the Baltic Proper. In the wake of such deep inflows, however, enhanced mixing accelerates thermohaline homogenisation on a wide range of spatio-temporal scales. In detail, the contributing mechanisms are still unclear, but may originate from externally/internally triggered processes. For instance, the spectra of long-term current records made over the eastern topographic flank of the Eastern Gotland Basin (EGB) showed a significant energy gap at a period of about 18 days (Hagen & Feistel 2004). This time scale may be considered to be the regional threshold for internally generated current fluctuations of shorter periods. Two significant peaks dominate this period range. The first of them corresponds to the so-called synoptic cycle with periods between 3 and 5 days due to quasi-rhythmic changes in actual weather conditions. The second one exhibits an accumulation of kinetic energy for a period of about 10 days; this is probably caused by corresponding changes in prevailing zonal winds. Both periods have already been discussed by Fennel & Lass (1982). These authors used a very much simplified analytical model to study associated fluctuations of the motion field within a rectangular basin of gently sloping bottom topography filled with homogeneous water. Simulated current fluctuations reflected basin-scale modes of resonantly released free, coastally trapped, barotropic waves. Associated anomalies in sea level propagated cyclonically around the basin. Their phase velocities were estimated to be 0.83 m s^{-1} (5 days, first mode) and 0.22 m s^{-1} (10 days, second mode). Comparable propagation velocities were reported for wave-like current fluctuations under stratified conditions by Aitsam & Talpsepp (1982) and Pizarro & Shaffer (1998). They analysed several-days-long current records in the context of hydrographic measurements and concluded that wind-forced subinertial waves are useful in interpreting actual motion dynamics on the scale of several days. Such waves may be the source of the lateral and vertical current meanders detected in the deep EGB by Hagen & Feistel (2004). Associated fluctuations generate changes in the vertical current shear and affect thermohaline mixing within the near-bottom layers, especially over the steep topographic mid-slope zone. Furthermore, there is some observational evidence that occasionally

occurring current instabilities generate eddy-like features with a diameter of several kilometres and a lifetime between days and few weeks within intermediate layers (see Elken et al. 1988, Reißmann 2005). Their trigger mechanisms are still unclear, but they could be related to abruptly changing wind conditions. The present study therefore focuses on two questions: (i) Is there observational evidence for such wave-like changes in the deep mass and current fields of the EGB as a result of occasionally changing winds, and (ii) what consequences must be expected for actual estimates of deep volume transports derived from geostrophic currents via hydrographic snapshot surveys?

2. Data base and methods

The Leibniz Institute for Baltic Sea Research Warnemünde (IOW) carried out a cruise on board r/v 'A. v. Humboldt' in the EGB from 18 April to 03 May 2000 (Fig. 1). All station positions were determined by satellite navigation (GPS) with an uncertainty in the range of decametres. However, they could be controlled indirectly by continuously echo-sounded water depths with an overall error of a few metres. This uncertainty in
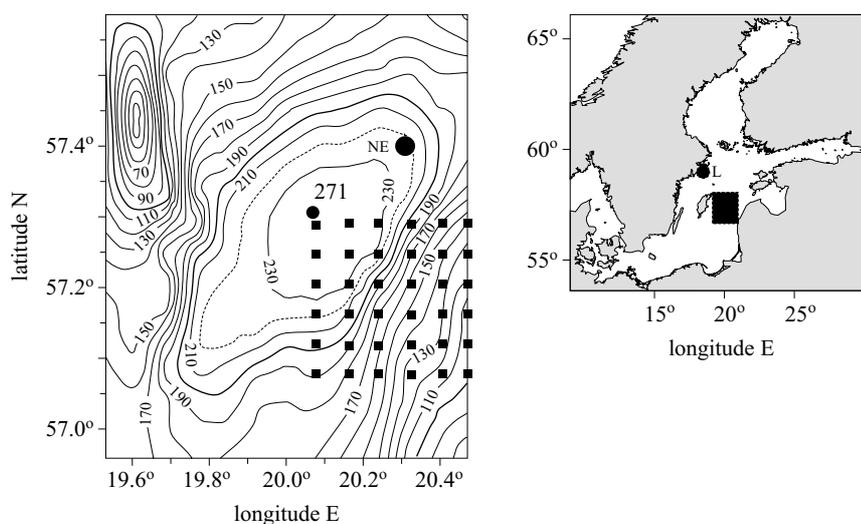

Fig. 1. Area of investigation in the Baltic Sea (rectangle) and location of the Swedish coastal station of Landsort (L, right panel); bathymetric map (in metres) of the Eastern Gotland Basin with the mooring position NE in the north-east and the central station 271 of the HELCOM monitoring programme (dots); hydrographic stations of the snapshot survey (squares) were profiled along zonal sections with a section/station spacing of 4.6 km; measurements started in the north-east and ended in the south-east from 19 to 20 April 2000 (left panel)

positions results mainly from actual fluctuations in the filling level of the Baltic Proper. Such changes are sufficiently described by the sea level anomalies observed at the Swedish coastal station of Landsort (Fig. 1). Daily sea levels at this station were provided by the Swedish Meteorological and Hydrological Institute. Standard meteorological parameters, such as air temperature, air pressure, wind direction and wind speed, were measured continuously on board. Their sampling interval was 1 minute at about 8 m above the sea surface. Wind vectors were decomposed into zonal (U = positive eastward) and meridional components (V = positive northward). Finally, hourly and/or daily averages of both wind components were used for further analyses.

The whole field campaign was carried out above the basin's steep southeastern topographic flank (Fig. 1). Here, the local Coriolis frequency is $f = 1.225 \times 10^{-4}$ (s^{-1}) with inertial period $T_f = 2\pi/f = 14.25$ h at a mean
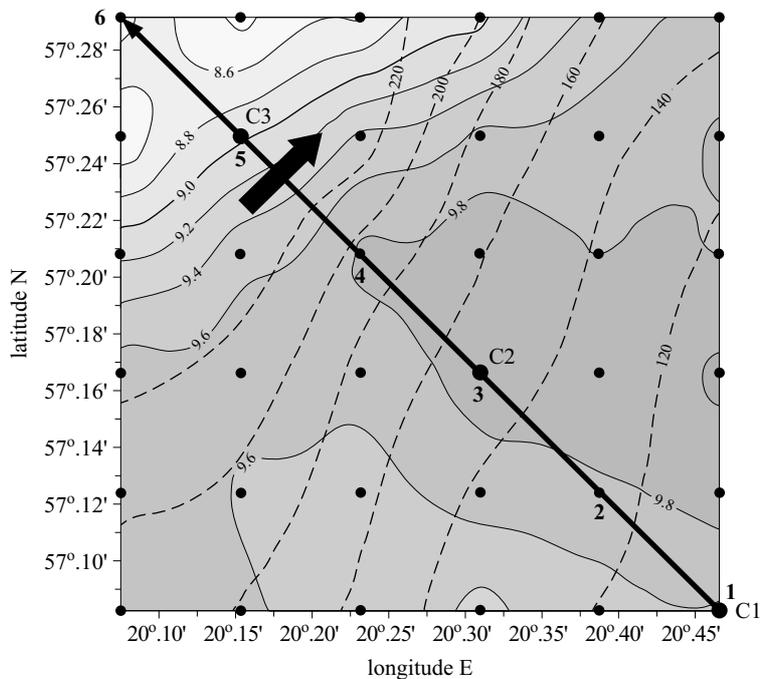

Fig. 2. Salinity patterns [PSU] at the pressure level of 80 dbar (grey) suggest an overall geostrophic (baroclinic) north-east current (arrow) following echo-sounded depths (broken lines, metres). The hydrographic snapshot survey covered 6×6 stations (dots) while the diagonal transect (bold line) represents six stations (1–6) with a spacing of 6.5 km; it was repeated 40 times with a sampling interval of 6 hours; each repeat started in the south-east (station 1) and ended in the north-west (station 6) between 20 April and 1 May 2000

Table 1. String abbreviation, position, echo-sounded water depth (H), target horizon (Z) of recording current meters (Aanderra-RCM) and SeaBird T–S recorder (SBE16) deployed at the three subsurface moorings denoted C1, C2, C3 in Fig. 2; the uniform sampling interval of all devices was 2 minutes; the top of each string was placed at 75 m depth

String	Lat. [N]	Long. [E]	H [m]	Z [m]	Start [UTC]	End [UTC]	Type
C1	57°05′	20°28′	102	90	19.04.2000 15:46	29.04.2000 06:30	RCM-9
				95	20.04.2000 00:00	29.04.2000 06:00	SBE16
C2	57°10′	20°18.6′	152	90	19.04.2000 16:40	29.04.2000 07:54	RCM-9
				115	19.04.2000 00:00	29.04.2000 08:00	SBE16
				140	19.04.2000 16:40	29.04.2000 07:54	RCM-9
				145	19.04.2000 00:00	29.04.2000 08:00	SBE16
C3	57°15′	20°09.3′	237	90	19.04.2000 18:00	30.04.2000 12:16	RCM-7
				115	19.04.2000 00:00	30.04.2000 12:00	SBE16
				140	19.04.2000 18:00	30.04.2000 12:16	RCM-7
				165	19.04.2000 00:00	30.04.2000 12:00	SBE16
				190	19.04.2000 18:00	30.04.2000 12:16	RCM-7
				215	19.04.2000 00:00	30.04.2000 12:00	SBE16
				230	19.04.2000 18:00	30.04.2000 12:16	RCM-7
				235	19.04.2000 00:00	30.04.2000 12:00	SBE16

latitude of 57°09′N. Three subsurface moorings (C1, C2 and C3) were deployed (see Fig. 2 and Table 1). Each of them was equipped with recording current meters and temperature sensors (Aanderra Recording Current Meter/RCM). In between their measuring horizons, several SeaBird recorders SBE-16 were mounted to obtain continuous records of temperature and salinity. The sampling interval of all the moored devices was two minutes. Current direction and current velocity were also decomposed into cross- (u, positive upslope to the south-east) and along-slope components (v, positive along-slope to the north-east). Thus, the usual co-ordinate system was negatively rotated by 45° at mooring sites C1 and C3, but by 25° at string C2. Hourly averages and hourly variances (σ_u^2, σ_v^2) were computed for these current components. The variances obtained provided the basis for estimates of the so-called 'eddy kinetic energy' per unit mass $EKE = (\sigma_u^2 + \sigma_v^2)/2$. This quantity is invariant versus any rotation of the co-ordinate system and describes the energy level of current fluctuations with periods shorter than one hour. Using the hourly averages, daily averages and daily standard deviations were computed for further analyses.

The hydrographic measurements started with a snapshot survey of the mass field on 19–20 April 2000 (Fig. 2). The station spacing was 4.6 km along six zonal sections separated meridionally by the same distance. Each section covered six hydrographic stations starting in

the north-east and ending in the south-east. Normal to the isobaths, the routine measurements followed the embedded diagonal transect of six stations spaced by 6.5 km. This station spacing was insufficient to resolve patterned mass field structures smaller than 13 km and prevented a serious discussion of smaller eddy-like features. Such phenomena should be dynamically trapped at the scale of the first mode radius of deformation. In the EGB, it reaches typical values between 5 and 8 km (Fennel et al. 1991). Therefore, the hydrographic analysis was limited to larger mass field patterns passing the section plane during the ten-day field campaign. The diagonal transect was repeated 40 times. Each repetition started at position 1 (string position C1) in the south-east and ended in the north-west, in the vicinity of the central station 271 of the HELCOM monitoring program (Fig. 1). The constant time step between successive transects was 6 hours (Table 2). It excluded all fluctuations with periods shorter than half a day, but it resolved fluctuations of the local inertial period to a sufficient extent.

Table 2. Numbers of hydrographic stations and abbreviations of current meter strings deployed in their vicinity, position, overall water depth <H> with associated standard deviation (STD) in metres, pressure range ΔP of CTDO-profiles digitised in 1 dbar steps, overall profile length (h), and resulting section distance (L) of the 40 times repeated diagonal transect shown in Fig. 2

Station	Lat. [°N]	Long. [°E]	<H> $\pm$ STD	ΔP [dbar]	h	L [km]
1∼(C1)	57.083	20.467	101 $\pm$ 0.7	3–100	97	0
2	57.125	20.390	131 $\pm$ 0.2	3–129	126	6.48
3∼(C2)	57.167	20.310	151 $\pm$ 0.6	3–150	147	12.96
4	57.208	20.233	196 $\pm$ 1.3	3–198	195	19.45
5∼(C3)	57.250	20.155	237 $\pm$ 0.2	3–234	231	25.93
6	57.292	20.075	241 $\pm$ 0.2	3–238	235	32.41

At each station, conductivity (C)/salinity (S), temperature (T), pressure (P)/depth (D), and dissolved oxygen (O_2) were profiled by using a standard SeaBird CTDO probe lowered from the near-surface to the near-bottom layers. Its temperature sensor was controlled by two reversing thermometers at different depths, at least twice along each transect. Analogous procedures were applied to the salinity with the aid of salinometer measurements. Dissolved oxygen was calibrated via the well-known Winkler method, while the pressure sensor was checked by the actual air pressure at the sea surface. The remaining mean errors are ± 0.014°C for temperature, ± 0.001 PSU for salinity, ± 0.029 cm^3 dm^{-3} for dissolved oxygen, and ± 0.043 dbar for pressure. After the necessary data validation, all vertical profiles

were digitised by pressure steps of 1 dbar. The potential density (PD) was computed with the reference level at the sea surface by applying the algorithms proposed by Feistel & Hagen (1995). Finally, the overall averages <S>, <T>, <O2>, and <PD> were computed for each pressure level at each station. They were subtracted from the original series to obtain corresponding anomaly series S', T', O2', and PD', respectively. Because the S' corresponds well to the PD' in the Baltic Sea, the spatio-temporal fluctuations in stratification were studied by empirical orthogonal functions resulting from the pressure-time matrix of the S'. This method is described in more detail in Wilks (1995). In general, it reduces a given data set of a certain number of variables to a new data set containing fewer variables (empirical modes), which represent a large fraction of the total variability of the original data. The resulting eigenfunctions are dimensionless and describe salinity/stratification anomalies in the pressure-section plane, whereas the corresponding coefficients mirror their temporal variability. The product of spatial eigenfunction and temporal coefficients yields the sign needed to interpret spatio-temporal changes physically.

3. Results

3.1. Local winds

The eleven-day field campaign was conducted entirely under moderate winds, although the prevailing sector did change significantly. This follows from ship-borne wind records, which show south-easterlies during the first five measuring days (Fig. 3). These winds pushed near-surface waters towards the Baltic Proper and the sea level increased at Landsort until 25 April (day of the year, DOY = 116). This wind sector was attributed to the western flank of a high air pressure bridge over the eastern Baltic Sea (DWD 2000). An atmospheric anticyclone over Scandinavia changed the wind sector over the study area for the remainder of the time. Along its south-eastern flank, the north-easterlies pushed near-surface waters from the Baltic Proper towards the south-western Baltic Sea. Consequently, the sea level decreased at the Landsort station.

3.2. Background conditions

3.2.1. Stratification

The major inflow of unusually warm, saline, but poorly oxygenated water during the winter of 1997–1998, which is described in more detail in Hagen & Feistel (2001), established exceptionally warm deep water in
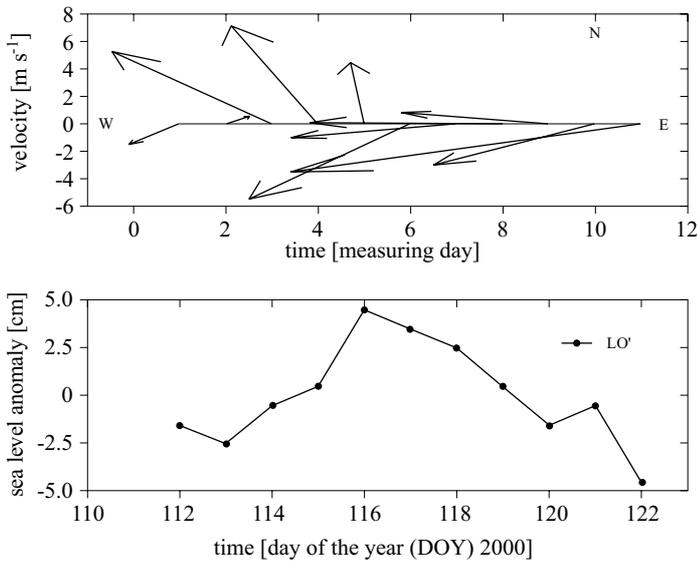
Fig. 3. Arrows of daily ship winds and corresponding anomalies in sea level observed at the Swedish coastal station of Landsort (LO') (see Fig. 1), from 21 April (day of the year DOY = 112) to 1 May 2000 (DOY = 122)
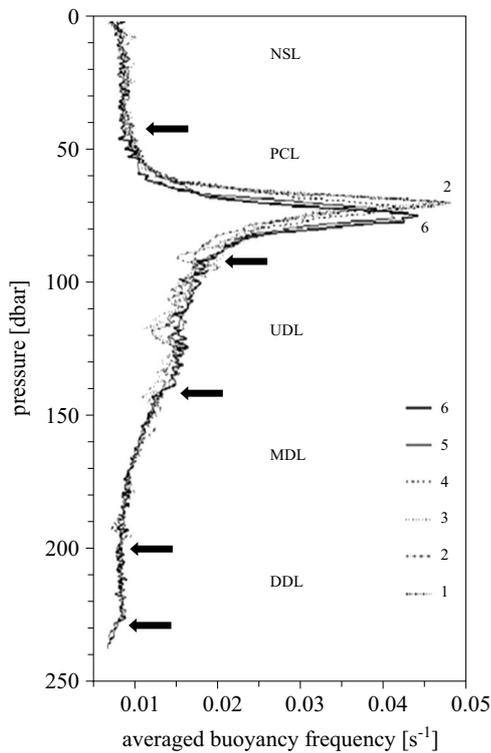

Fig. 4. Overall vertical profiles [dbar] of the Väisälä-frequency <N> at the six stations (1–6) along the diagonal transect shown in Fig. 2; the recorded stratification conditions were classified in the form of five sub-layers: the near surface layer (NSL), the pycnocline layer (PCL), the upper (UDL), the middle (MDL), and the deepest deep layer (DDL) (see Table 3)

Table 3. Section characteristics of the five sub-layers identified in Fig. 4, their denotations and abbreviations, pressure/depth range $<\delta P>$, sub-layer thickness $<h^*>$ (1 dbar $\sim$1 m), and layered buoyancy frequency $<N^*>$

Sub-layer	No.	Symbol	$<\delta P>$ [dbar]	$<h^*>$ [m]	$<N^*>$ $[s^{-1}] \times 10^3$
near-surface	1	NSL	3–40	37	8.61 ± 0.56
pycnocline layer	2	PCL	41–90	49	19.72 ± 10.61
upper deep layer	3	UDL	91–140	49	15.58 ± 1.85
middle dep layer	4	MDL	141–200	59	10.21 ± 1.63
deepest deep layer	5	DDL	201–238	37	8.13 ± 0.57

the EGB. The next relevant inflow event occurred in October 2001 (Feistel et al. 2003). Consequently, our ten-day field campaign was conducted entirely during a so-called stagnation period with well-stratified deep water. Stratification is usually described by changes in the vertical density profile expressed by the squared buoyancy frequency $N^2 = -(g/\rho_o)(\Delta\rho/h')$. Here, the acceleration due to gravity is $g = 9.81$ m s^{-2}, and the averaged density between two selected isopycnal surfaces is ρ_o. In the search for characteristic conditions in stratification and with the application of pressure steps of 1 dbar $\sim h' = 1$ m for the computation of the density difference $\Delta\rho$, the temporally averaged profiles of the buoyancy frequency $<N>$ are plotted for each station in Fig. 4. Corresponding plots of the salinity $<S>$, temperature $<T>$ and dissolved oxygen $<O2>$ (not shown) suggest that the background stratification can be characterised by the following five sub-layers:

(i) The near-surface layer (NSL), filled with well-oxygenated, but relatively warm brackish water down to c. 40 dbar.

(ii) The halocline/pycnocline layer (PCL), marked by pronounced vertical gradients in all three hydrographic quantities between 40 and 90 dbar; peak values mark its core at a pressure level of c. 75 dbar.

(iii) The upper deep layer (UDL), which revealed exponentially increasing salinities and temperatures, but only traces of dissolved oxygen between 90 and c. 140 dbar.

(iv) The middle deep layer (MDL), where conditions were totally anoxic. Both salinity and temperature increased linearly between 140 and c. 200 dbar.

(v) The deepest deep layer (DDL), filled with extremely warm, saline water enriched with relatively high concentrations of hydrogen sulphide below a pressure level of 200 dbar.

3.2.2. Deep circulation

On inspecting Fig. 4 in somewhat more detail, it becomes clear that the overall core depth of the PCL was deeper at station 6 than at the first two stations, roughly by $<\delta h^*> \sim 5.5$ m. This along-section inclination of the pycnocline core suggests that relatively dense water persistently ascended from deep layers into the PCL to maintain an internal high pressure belt over the basin's eastern rim. Associated pressure gradients towards the basin's centre obviously balanced a baroclinic north-east current. However, this overall inclination of the PCL points indirectly to an opposite gradient in the sea level maintaining a barotropic south-west current. Because the adjustment time of barotropic currents is much shorter than that of baroclinic currents, the two geostrophic components rarely cancel each other at a given time (Csanady 1982). In other words, we may expect persistently released adjustment processes between barotropic and baroclinic motion modes. Following Allen (1980), the barotropic fraction of along-slope currents should be topographically trapped on the scale $<\gamma> = <H> / <\alpha>$. This results from the typical water depth $<H>$ and the characteristic bottom slope $<\alpha>$. On inserting the water depths from Table 2, we find the mean topographic slope between stations 6 and 1 to be $<\alpha> = (241 - 101)$ m $/$ 32.41 km $= 4.32 \times 10^{-3}$. Along all six stations, the overall water depth is $<H> = 176$ m. Thus, the estimated $<\gamma> = 41$ km exceeds the section length of 32.5 km by about 20%. In contrast, the geostrophically adjusted component of baroclinic currents should be trapped on the much smaller scale of the first mode radius of deformation $R_{bc} = (N \times h)/f$ (Pedlosky 1979). Here, $N = <N_{tot}>$ is the total buoyancy frequency averaged temporally/vertically for each profiling depth (h) of each station position listed in Table 2. The $<R_{bc}>_{num}$ were computed numerically as proposed by Klinck (1999, http://woodshole.er. usgs.gov/operations/sea-mat/klinck-html/dynmodes.html).

Both $<N_{tot}>$ and $<R_{bc}>_{num}$ are given together with resulting section averages in Table 4. To a certain degree, the ratio $\beta = <R_{bc}>_{num} / <\gamma>$ reflects the coupling between baroclinic and barotropic current dynamics. It varies between 0 (no coupling) and 1 (complete coupling). Station values fluctuate between $\beta = 0.12$ (station 1) and $\beta = 0.27$ (station 6). This suggests that such a coupling increased towards the basin's centre, roughly by a factor of two. Hypothetically decomposing the geostrophic fraction of deep currents into baroclinic and barotropic components, the obtained values of β suggest that the barotropic component dominated along the whole transect. Consequently, it could be expected that multi-day changes in deep currents and associated volume transports react immediately to fluctuations in sea level gradients caused by changed wind conditions.

Table 4. Total buoyancy frequency $<N_{tot}>$ averaged temporally/vertically over the profiling depth (h) at each station position (Table 2) and numerically computed first mode radii of deformation $<R_{bc}>_{num}$; the last column contains the section means

		Station No.						Mean
		6	5	4	3	2	1	
$<N_{tot}> \times 10^3$	$[s^{-1}]$	5.68	5.73	6.16	6.75	6.90	6.69	6.32
$<R_{bc}>_{num} \sim <N_{tot}\,h>/f$ [km]		10.9	10.8	9.8	8.1	7.1	5.3	8.7

According to Soomere (2001), the extent of associated wind patterns dramatically exceeds the length of the diagonal transect.

3.2.3. Water masses

By definition, characteristic water masses are mirrored by a dot in the temperature (T) – salinity (S) diagram (Mamayev 1975). Plotting all T–S profiles of each station, it becomes clear that both the near-surface and the superficial layers were occupied by brackish water (BW) (Fig. 5). Their temperatures fluctuated between 4° and 7°C, whereas the salinity was only slightly in excess of 7 PSU. The well-known Baltic Winter Water (BWW)
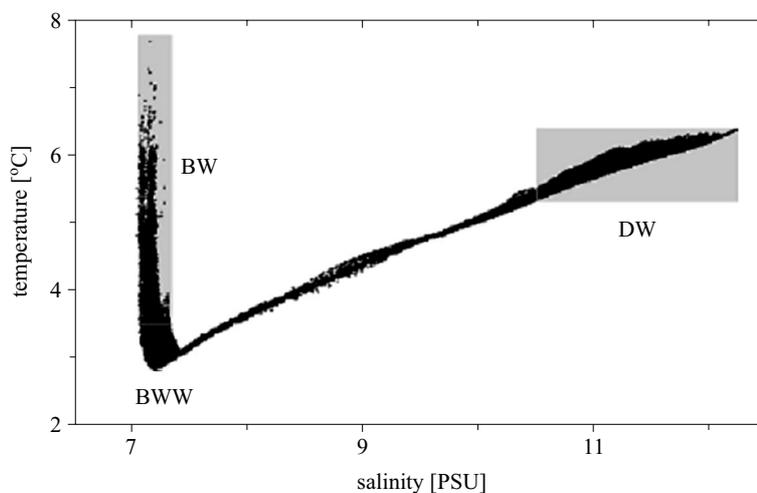

Fig. 5. Overall temperature [°C] – salinity [PSU] diagram resulting from repeated profiles at the stations 1–6 of the diagonal section (see Fig. 2 and Table 2); the scatter exhibits brackish water (BW, shaded grey) in the upper layers, the cold Baltic Winter Water (BWW) above the perennial pycnocline, and the warm and saline deep water (DW); note the quasi linear T–S relationship between the BWW and the DW suggesting thermohaline mixing of constant intensity within the deep layers
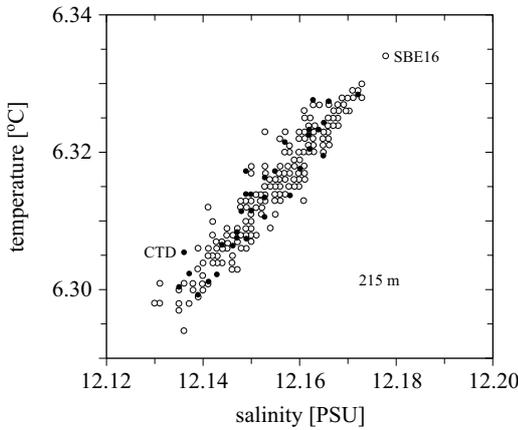
Fig. 6a. Temporal temperature [°C] – salinity [PSU] diagram resulting from N = 252 hourly averaged records of the SBE16 recorder deployed at 215 m depth at the mooring site C3 (open circles) and that of N = 35 consecutive standard hydrographic measurements carried out with a sampling interval of 6 hours at a pressure level of 215 dbar at station 5 from 20 to 30 April 2000 (dots) (see Fig. 2)
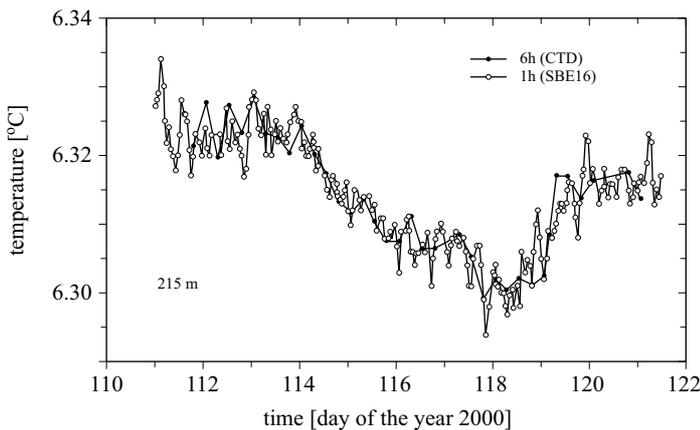

Fig. 6b. Temperature series [°C] of data scattered in Fig. 6a

exhibited the lowest temperatures, just above the PCL. In the deeper layers, the thermohaline properties of the BWW were mixed persistently with those of relatively warm and saline deep water (DW). This resulted, for instance, in a quasi-linear T–S relationship between (3–6)°C and (7.5–12) PSU in the hourly averages of the SBE-16 recorder. It was deployed at 215 m depth of the moored string C3 (Fig. 6a). The corresponding scatter plot from the CTD standard measurements was based on six hourly repeats at station 5 (C3). Both scatters coincide sufficiently well. This is confirmed

by the resulting temperature curves plotted in Fig. 6b. Retroactively, the
detected synchrony in differently sampled temperature series confirms that
aliasing was not a serious problem for the deep hydrographic standard
measurements.

3.3. Multi-day variability

3.3.1. Stratification

Overall averages have been subtracted from the original profiles to
obtain the temporal anomalies S', T', and O2' for each pressure level
at each station. The largest temporal variability in salinity/stratification
was observed within the PCL, especially over the topographic mid-slope
zone (not shown). It decreased significantly towards deep layers as
well as towards the basin's centre. To study the multi-day variabil-
ity in salinity anomalies, the pressure-time matrix of the S' was de-
composed into empirical orthogonal functions. Their first two modes
(n = 1, 2) explain more than 64% of the overall variance (Table 5).

Table 5. Eigenvalues of the first two empirical modes (n) of the salinity anomaly
(S') at stations 6–1; their contribution to the total variance is given in brackets

n	Station No.					
	6	5	4	3	2	1
1	46.7	48.0	60.2	49.4	37.8	40.6
2	16.8	21.3	14.5	15.7	32.1	26.0
Sum [%]	(63.5)	(69.3)	(74.7)	(65.1)	(69.9)	(66.6)

Consequently, we would like to focus our attention on the spatio-temporal
structures of these two modes in the following. Their along-section eigen-
functions describe vertically patterned stratification conditions (Fig. 7).
First-mode structures exhibited the PCL over an along-section distance
of about 20 km. The PCL occupies the layer between 60 and 110 dbar
and belongs to the chessboard-like patterns characterising the entire section
plane. Such persistent mass field structures can only be maintained by
intermediately alternating intrusions of more or less saline water. This
follows from the contoured time coefficients. Their alternating sign exhibits
wave-like fluctuations with a quasi-period of about 9 days. Associated
anomalies propagated with a speed of about $32 \, \mathrm{km} \, / \, 9\mathrm{d} = 0.04 \, \mathrm{m \, s^{-1}}$ towards
the basin's centre. This is confirmed by vertically averaged anomalies of
both the salinity <S'> and the temperature <T'> between pressure levels
of 70 and 80 dbar (Fig. 8). Over the topographic mid-slope zone, the
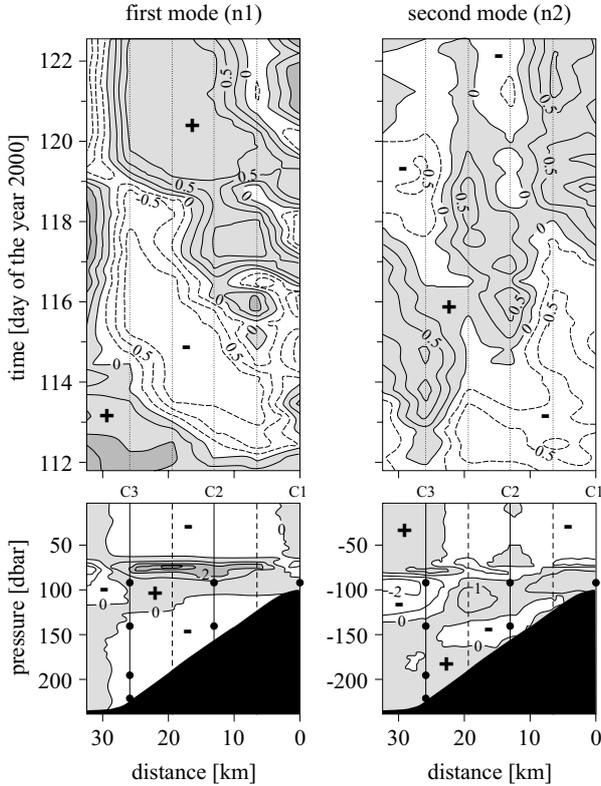
Fig. 7. Contours of the first two empirical modes (n1, n2) of salinity anomalies (S') resulting from the diagonal transect repeated 40 times between day of the year DOY = 112 (21 April) and DOY = 122 (1 May 2000) (see Fig. 2 and Table 5):

– upper panel: time coefficients with positive values shaded grey, dotted vertical lines show the station positions,

– lower panel: eigenfunctions within the section plane with the mooring positions C1, C2, and C3 (vertical lines) and measuring horizons of the RCM (dots) (see Table 1); additional positions of the hydrographic stations are given by vertical dashed lines

earlier intrusion of fresh and cold water was displaced by one of saline and warm water. After day 115, for instance, the pressure level of the 9 PSU surface, P(S = 9 PSU), shifted synchronously to shallower depths to form an internal frontal zone of large lateral gradients. It separated the thermohaline characteristics of the central basin from those of the basin's rim and migrated towards the basin's centre, too. The embedded core of baroclinic along-slope currents followed this overall front displacement. On the other hand, the second stratification mode exhibited much more complicated structures, not only along the section plane but also in time.
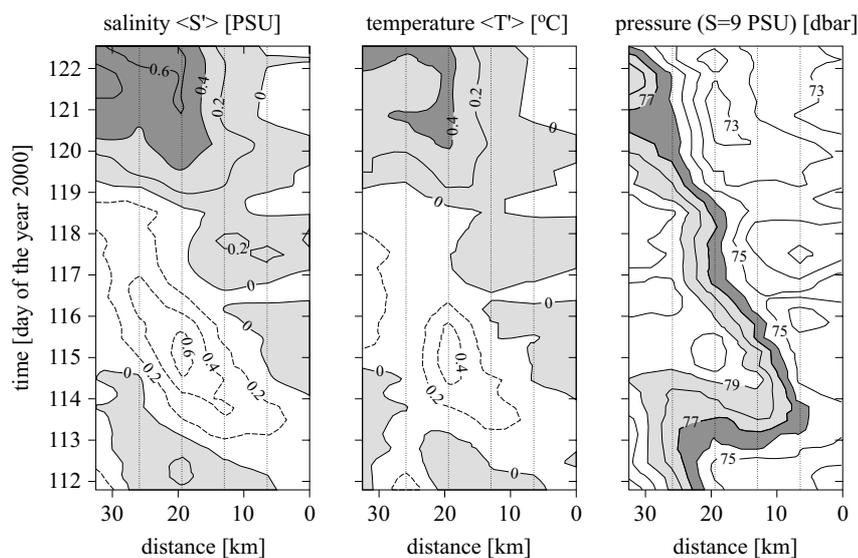
Fig. 8. Vertically averaged anomaly contours (70–80 dbar) of the salinity $<S'>$ and the temperature $<T'>$ with grey positive values along the diagonal transect as in Fig. 7; the right-hand panel shows the corresponding pressure levels of the 9 PSU isohaline surface with steep along-section gradients between 76 and 79 dbar, exhibiting the core displacement of embedded geostrophic along-slope currents towards the basin's centre

For instance, it exhibited a layer of positive eigenfunctions following the topographic slope (lower right panel in Fig. 7). The sign of related time coefficients alternated and the displacement of peak values suggested a mean propagation speed of about 32 km / 4d or 0.09 m s^{-1} towards the basin's rim. This means, however, that both stratification modes involved opposite propagation directions and their displacement velocity differed by a factor of about two. Nevertheless, all these findings confirm that wave-like processes modify the deep cyclonic background circulation on a synoptic scale.

3.3.2. Deep rim current (DRC)

Table 6 lists the basic statistics of the deep along-slope current on the basis of hourly averages. The core of the deep rim current (DRC) was present in both the MDL and the DDL. Its mean velocity exceeded 0.02 m s^{-1}, just above the topographic mid-slope where the greatest short-term variability occurred (Fig. 9). The latter has been expressed by the so-called eddy kinetic energy (EKE). Sub-layers of extremely short-term variability in the deep current point indirectly to enhanced mixing

Table 6. Basic statistics of hourly along-slope currents resulting from the three mooring sites C1, C2, and C3 described in Table 1; corresponding curves are plotted in Fig. 10 for N hours (h) with the median (Med.), mean, variance (Var.), skewness (S), kurtosis (K), maximum (Max.), minimum (Min.), and resulting fluctuation range (Max.-Min.)

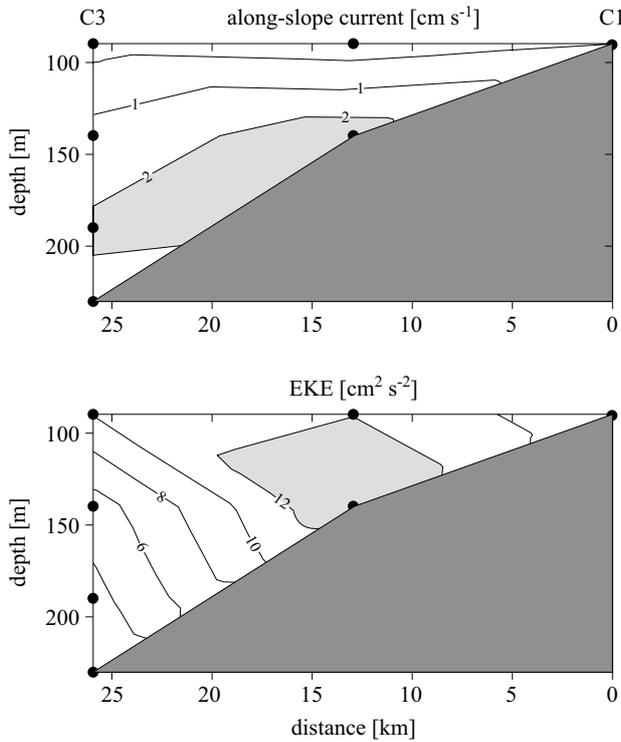| Site	N	Med.	Mean	Var.	S	K	Max.	Min.	Range
	[h]	$[\text{cm s}^{-1}]$		$[\text{cm s}^{-1}]^2$			$[\text{cm s}^{-1}]$		
C1	229	-0.26	-0.01	7.81	0.11	-0.52	7.06	-6.04	13.10
C2	231	1.72	2.21	17.08	0.41	-0.51	12.49	-6.34	18.83
C2	231	2.66	2.65	21.80	-0.04	-0.83	12.19	-6.70	18.89
C3	258	-0.29	-0.26	11.38	0.27	1.81	11.21	-10.18	21.39
C3	258	1.07	1.31	4.65	0.32	1.18	8.41	-5.25	13.66
C3	258	2.19	2.11	2.31	-0.32	0.79	6.16	-3.83	9.99
C3	258	1.10	1.48	1.69	0.70	0.37	5.35	-0.97	6.32

Fig. 9. Overall velocity of the deep rim current following the isobaths towards the north-east between mooring sites C1 and C3 with core speeds > 2 cm s^{-1} (grey, upper panel) (see Fig. 2 and Table 6); the lower panel shows the corresponding contours of the eddy kinetic energy per unit mass (EKE, cm^2 s^{-2}) with peak values above the topographic mid-slope zone
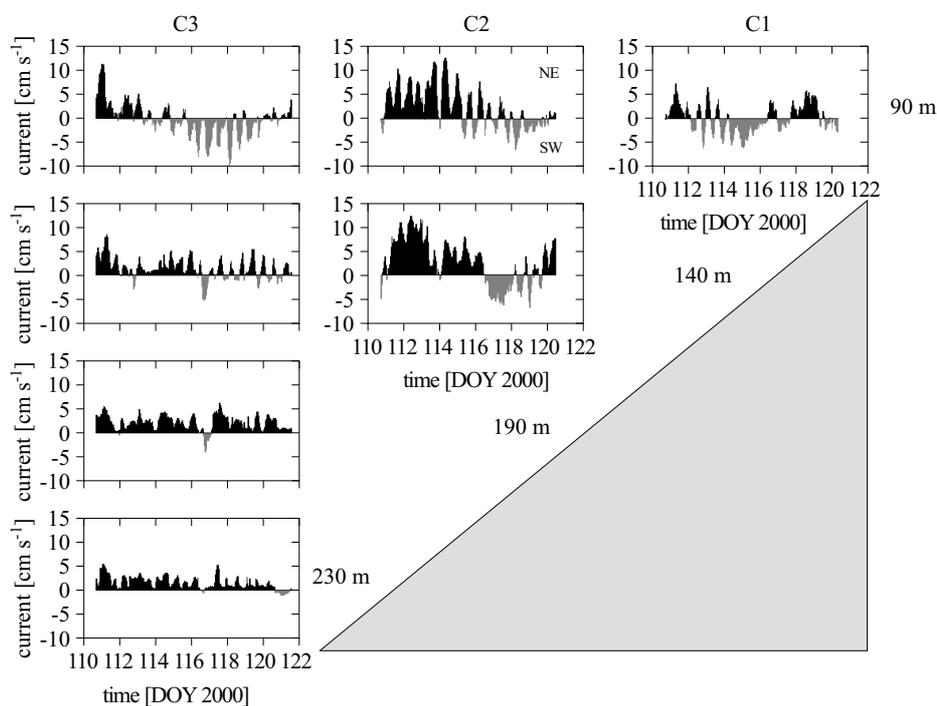
Fig. 10. Time series of hourly along-slope currents (black towards the north-east, NE) resulting from the mooring sites C1, C2, and C3 between days of the year DOY = 111 and 121 (19–30 April) (see Fig. 2 and Table 6); short-term fluctuations of all measuring horizons can be attributed mainly to the local inertial period of about 14 hours, while multi-day changes with a period of about 10 days characterise along-slope motions between 90 and 140 m depth over the topographic mid-slope zone (C2), where the tendency for south-westward deep rim currents (SW) started on DOY = 116

conditions, which may be maintained by the vertical current shear or breaking inertial waves. Towards the sea bed, however, the power spectra of all current components revealed decreasing energy levels for the local inertial period at each moored string (not shown). Thus, we may speculate that near-bottom mixing is controlled essentially by the vertical current shear accompanying lateral/vertical meanders of the DRC. Owing to the detected enlargement of the EKE above the topographic mid-slope zone, we would like to examine the current records of string C2 (see Fig. 2). Here, the quasi ten-day cycle produced fluctuations within the layers between 90 and 140 m depth (Fig. 10). At 90 m depth, just beneath the PCL, positive currents reflect enhanced north-eastward motions advecting less saline and cooler water through the section plane until day 116 (see Figs. 7 and 10). However, day 116 also reflects the change in the prevailing wind sector
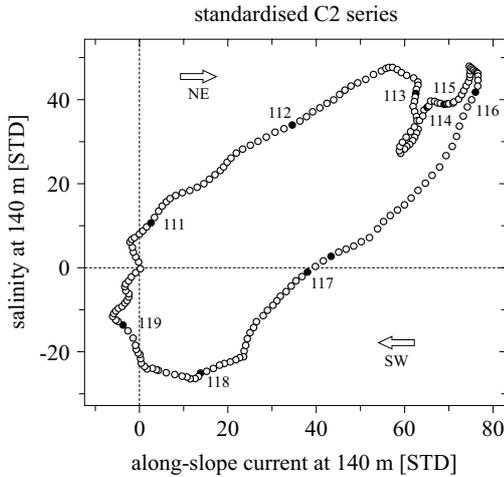
standardised C2 series

Fig. 11. Cumulatively plotted series (mean = 0, standard deviation STD = 1) of the hourly along-slope current recorded at 140 m depth (positive towards the north-east) and the corresponding salinity series of the SB16 recorder deployed at 145 m depth of the string C2 (very near the hydrographic station 3, cf. Fig. 2); filled circles mark the particular noonday; note that the north-eastward advection of saline deep water (NE, arrow pointing to the right) was replaced definitively by the south-westward advection (SW) of fresher water at the beginning of DOY = 116 (25 April)

(Fig. 3). Thus, it represents the 'turning day' between the prevailing positive (north-eastward) and negative (south-westward) along-slope motions in the deeper layers. This becomes evident from the cumulatively scattered series of standardised (mean = 0, standard deviation STD = 1) along-slope currents versus corresponding anomalies at the salinity recorded at the 145 m horizon (Fig. 11). More insight into the reaction of the baroclinic fraction of the DRC to changed forcing conditions may be obtained from the time behaviour of its geostrophic component based on hydrographic profiles (Fig. 12). Day 116 terminated the first half-cycle of the detected quasi-period. Selecting the level of no motion to be at the sea surface, the baroclinic core velocity exceeded 0.07 m s^{-1} in the layers below 90 m depth. It covered a section distance of about 10 km above the topographic mid-slope zone. One day later, the core speed accelerated to more than 0.12 m s^{-1}. Simultaneously, the current core shifted towards the deeper layers near the centre of the basin. Its overall displacement velocity of 10 km / 4 d = 0.03 m s^{-1} retroactively confirms the magnitude estimated for the migration of the frontal zone within the PCL (see Figs. 7 and 8).
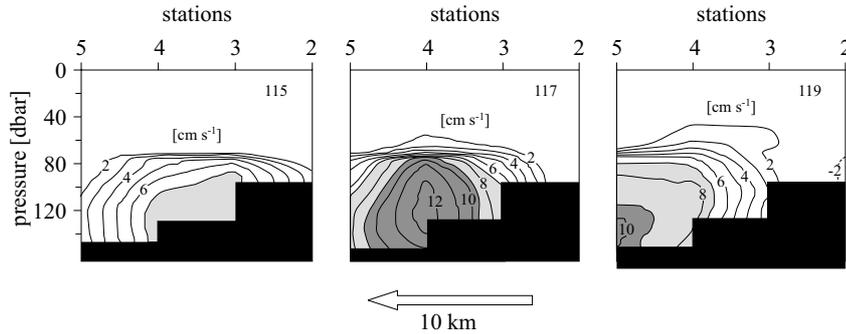
Fig. 12. Contours of geostrophic currents [cm s^{-1}] between stations 2 and 5 computed in two-day steps from hydrographic section repeats around the 'turning day' DOY = 116; adjacent values between stations 1–6 were averaged for smoothing and the level of no motion was selected to be at the sea surface for all three transects profiled between 17:00 and 21:00 UTC; resulting core speeds of north-eastward currents > 0.07 m s^{-1} are shaded grey; note the displacement of the deep current core towards the basin's centre

3.3.3. Deep volume transports

To a rough approximation, daily volume transports may be considered to consist of the sum of the baroclinic and barotropic components of geostrophic motions ($T_{obs} = T_{gbc} + T_{gbt}$). Observed estimates of T_{obs} result from spatial averages of the measured along-slope currents shown in Fig. 10. The overall velocity was multiplied by the corresponding along-section area $(6.500 \times 4 \times 145) / 2$ m$^2 \sim 1.9$ km^2 between strings C1 and C3. The plane of baroclinic currents was estimated at $(6.500 \times 3 \times 147) / 2$ m$^2 \sim 1.4$ km^2 between hydrographic stations 2 and 5. Because this area is smaller by a factor of about 0.7, all transports derived from the moored strings were multiplied by this factor for comparability. Further comparability was obtained by plotting standardised series (Fig. 13). Thus, it became clear that the daily T_{obs} originated mainly from the barotropic component (T_{gbt}). Both series were roughly in phase during the quasi ten-day cycle, but they were out of phase with those of the baroclinic geostrophic transport (T_{gbc}) by about 5 days. The latter essentially followed the filling level of the Baltic Proper as described by the Landsort sea level anomaly (LO'). Considering the eight consecutive days (DOY = 112–119), overall transports were $<T_{gbc}> = (4.8 \pm 0.6)$ km^3 d^{-1} and $<T_{obs}> = (1.2 \pm 0.5)$ km^3 d^{-1} towards the north-east. These values suggest, however, that there was a total barotropic south-westward transport of about $<T_{gbt}> = -3.6$ km^3 d^{-1}. This has to be balanced by negative anomalies of the sea level in the south-east and positive anomalies
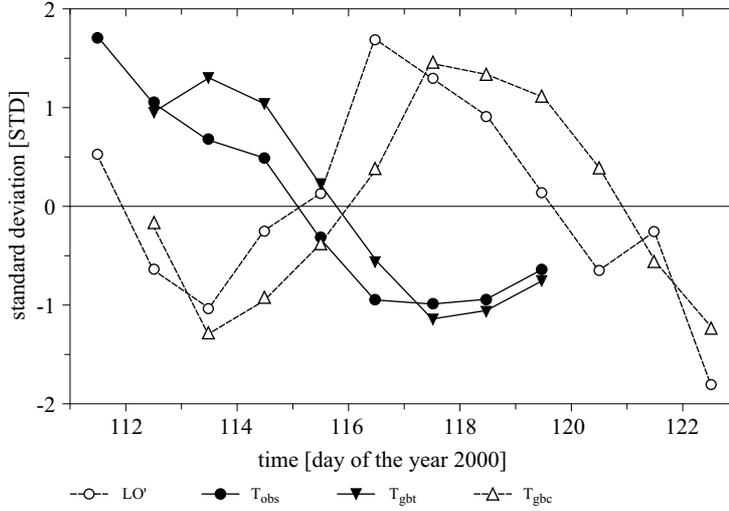
Fig. 13. Standardised daily anomalies (mean = 0, standard deviation STD = 1) of the sea level at the Landsort coastal station (LO', open circles) compared with the corresponding estimates of deep volume transports (T) passing the section plane beneath the pycnocline; comparable transports result from 8 consecutive days between DOY = 112 and DOY = 119:

- T_{obs} = observed from moored current meter strings C1, C2, and C3 (dots),
- T_{gbc} = geostrophically computed between stations 2 and 5 as shown in Fig. 12 (open triangles),
- $(T_{obs} - T_{gbc}) = T_{gbt}$ = expected fraction of the barotropic volume transport (filled triangles)

in the north-west, where the Landsort coastal station is situated. Subtracting the mean values, the linear regression between the Landsort sea level anomalies (LO') and T_{obs} shows a negative correlation (Fig. 14). The resulting coefficient of determination is $R^2 = 0.81$. Typical changes of +10 cm in the LO' released fluctuations in south-westward volume transport of about $T_{obs} = -5$ km^3 d^{-1}, and vice versa.

4. Discussion

Analysing the three-year current records during a perennial stagnation period in the deep waters of the EGB, Hagen & Feistel (2004) reported a persistent northward current with an overall velocity of about 0.03 m s^{-1} over its north-eastern topographic flank. Their mooring position is denoted by NE (57°23′N, 20°19.6′E) in Fig. 1. Here, the overall water depth is 224 m. Owing to the closed topographic contours, these measurements suggested
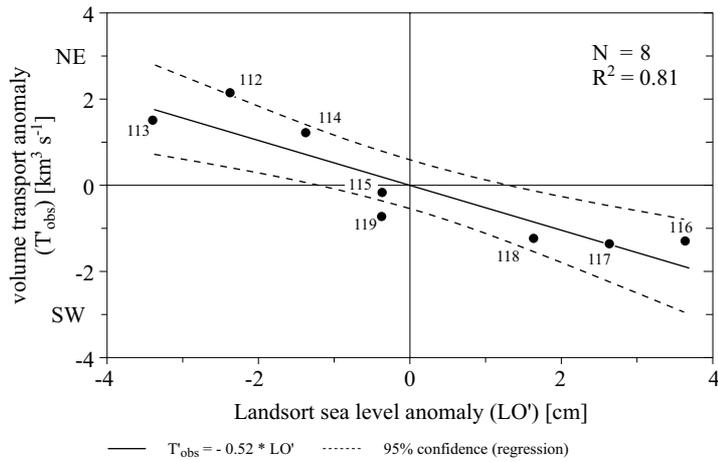
Fig. 14. Negative linear regression between daily anomalies in the Landsort sea level (LO') and corresponding changes in observed volume transports ($T'_{obs} > 0$ to the north-east, NE) passing the 90–230 m depth plane between the current meter strings C1 and C3 during N = 8 days (DOY = 112–119) in April 2000; the resulting coefficient of determination is $R^2 = 0.81$
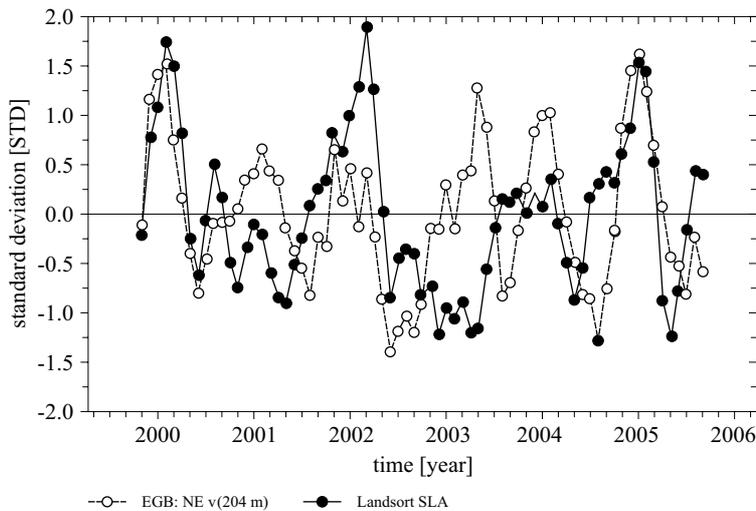

Fig. 15. Three-monthly running averages of standardised series (mean = 0, standard deviation STD = 1) of the Landsort sea level anomaly (SLA) reflecting changes in the filling level of the Baltic Proper and the along-slope currents (v) recorded 20 m above the sea bed at the mooring site denoted NE in Fig. 1; note the general similarity of both curves during so-called stagnation conditions, whereas considerable discrepancies point to other relevant dynamics during and after the strong inflow reported for the winter of 2002–2003

a persistent cyclonic circulation forming the topographically steered deep rim current (DRC). 20 metres above the sea bed, the core of the DRC commonly accelerates by a factor of about 2–3 during the winter season. The original current series started in August 1999 and was continued until October 2005. Most of the recording time was characterised by stagnant deep water conditions, which were dramatically interrupted by the cold inflow event during the winter of 2002–2003 (Feistel et al. 2006). On the basis of three-monthly running averages starting in September 1999 and ending in September 2005, it became clear that background changes in the strength of the cyclonic deep circulation react synchronously to those of the Landsort sea level (Fig. 15). Consequently, monthly changes in the deep circulation of the EGB can be described by the corresponding fluctuations in the filling level of the Baltic Proper. Following Samuelsson & Stigebrandt (1996), all long-term variations in the sea level of the Baltic Proper should be forced externally through corresponding fluctuations outside the Baltic Sea. However, wind-induced changes in sea level gradients across the Baltic Proper persistently modify the interaction between slow baroclinic and fast barotropic motion modes to produce characteristic changes in the deep circulation of the EGB on the synoptic scale of several days. This was confirmed by hydrographic and current measurements carried out over its eastern topographic flank during ten days in April 2000. Within the pycnocline layer (PCL), for instance, the reaction of baroclinic currents to changed wind conditions was characterised by:

(i) prevailing north-eastward motions accompanied by the intrusion of fresher/cooler water into the PCL, but the advection of more saline/warmer water into the deeper layers during the first five days, and

(ii) dominating south-westward motions accompanied by the intrusion of more saline/warm water into the PCL, but the advection of fresher/cooler water into deeper layers during the remaining time.

The embedded frontal zone, which separated the thermohaline properties of the slope water from those of the basin's centre, propagated with an averaged speed of about 0.04 m s^{-1} towards the centre of the EGB. This migration velocity corresponds to that of the cyclonic background circulation. At first glance, the observed front propagation confirms the cyclonically rotating double-cell circulation mirroring wind-forced topographic waves, as discussed for the Gulf of Riga by Raudsepp et al. (2003). However, the phase propagation of such wave types is expected to be several decimetres per second (see Clarke 1977, Csanady 1982, Pizarro & Shaffer 1998). In the near future, this discrepancy between the expected and detected propagation velocities of intermediately trapped wave-like

motions will be clarified in somewhat greater detail in that currently running versions of numerical circulation models will be used. Nevertheless, it did become evident that there was a straightforward reaction of barotropically steered changes in deep volume transports to synoptic changes in regional winds. In other words, it could be demonstrated that the practical account of baroclinic transport estimates from hydrographic snapshot surveys is quite useless for describing the daily changes in the water budget of the deep EGB.

Acknowledgements

References

Aitsam A., Talpsepp L., 1982, *Synoptic variability of currents in the Baltic Proper*, [in:] *Hydrodynamics of semi-enclosed seas*, Elsevier, Amsterdam, 469–488.

Allen J. S., 1980, *Models of wind-driven currents on the continental shelf*, Annu. Rev. Fluid Mech., 12, 389–433.

Clarke A. J., 1977, *Observational and numerical evidence for wind-forced coastal trapped long waves*, J. Phys. Oceanogr., 7 (2), 231–246.

Csanady G. T., 1982, *Circulation in the coastal ocean*, D. Reidel, Dordrecht, 279 pp.

DWD, 2000, *Bodenwetterkarte*, Amtsbl. Deut. Wetterdien.

Elken J., Pajuste M., Kouts T., 1988, *On intrusive lenses and their role in mixing in the Baltic deep layers*, Proc. 16th Conf. Baltic Oceanogr., Kiel.

Feistel R., Hagen E., 1995, *On the GIBBS thermodynamic potential of seawater*, Prog. Oceanogr., 36, 249–327.

Feistel R., Nausch G., Hagen E., 2003, *The Baltic inflow of autumn 2001*, Meereswiss. Ber., 54, 55–68, [http://www.io-warnemuende.de/documents/ mebe54_inflow01.pdf].

Feistel R., Nausch G., Hagen E., 2006, *Unusual Baltic inflow activity in 2002–2003 and varying deep-water properties*, Oceanologia, 48 (S), 21–35.

Fennel W., Lass H. U., 1982, *Phytoplankton patchiness and advection diffusion models*, Beitr. Meeresk., 47, 95–103.

Fennel W., Seifert T., Kayser B., 1991, *Rossby radii and phase speeds in the Baltic Sea*, Cont. Shelf Res., 11 (1), 23–36.

Gill A. E., 1982, *Atmosphere ocean dynamics*, Acad. Press, New York, 662 pp.

Hagen E., Feistel R., 2001, *Spreading of Baltic deep water: a case study for the winter 1997–1998*, Meereswiss. Ber., 45, 99–133, [http://www.io-warnemuende.de/research/mebe.html].

Hagen E., Feistel R., 2004, *Observations of low-frequency current fluctuations in deep water of the Eastern Gotland Basin/Baltic Sea*, J. Geophys. Res., 109, C03044, doi: 10.1029/2003JC002017.

Mamayev O. I., 1975, *Temperature-salinity analysis of world ocean waters*, Elsevier, Amsterdam, 374 pp.

Meier H. E. M., Kauker F., 2003, *Sensitivity of the Baltic Sea salinity to the freshwater supply*, Climate Res., 24 (3), 231–242.

Omstedt A., Axell L. B., 1998, *Modeling the seasonal, interannual, and long-term variations of salinity and temperature in the Baltic proper*, Tellus A, 50 (5), 637–652.

Pedlosky J., 1979, *Geophysical fluid dynamics*, Springer-Verlag, New York, 624 pp.

Pizarro O., Shaffer G., 1998, *Wind-driven, coastal-trapped waves off the Island of Gotland, Baltic Sea*, J. Phys. Oceanogr., 28 (11), 2117–2129.

Raudsepp U., Beletsky D., Schwab D. J., 2003, *Basin-scale topographic waves in the Gulf of Riga*, J. Phys. Oceanogr., 33 (5), 1129–1140.

Reißmann J. H., 2005, *An algorithm to detect isolated anomalies in three-dimensional stratified data fields with an application to density fields from four deep basins of the Baltic Sea*, J. Geophys. Res., 110, C12018, doi: 10.1029/2005JC002885.

Samuelsson M., Stigebrandt A., 1996, *Main characteristics of long-term sea level variability in the Baltic Sea*, Tellus A, 48 (5), 672–683.

Schinke H., Matthäus W., 1998, *On the causes of major Baltic inflows – an analysis of long time series – trends, errors and discontinuities*, Cont. Shelf Res., 18 (1), 67–97.

Soomere T., 2001, *Extreme wind speeds and spatially uniform wind events in the Baltic Proper*, Proc. Estonian Acad. Sci. Eng., 7, 195–211.

Wilks D. S., 1995, *Statistical methods in the atmospheric science: an introduction*, Acad. Press, San Diego, 464 pp.